Stem Cell Reports
Article

ISSCR

OPEN ACCESS

EVA1A/TMEM166 Regulates Embryonic Neurogenesis by Autophagy

Mengtao Li,[1,4] Guang Lu,[1,4] Jia Hu,[2,3,4] Xue Shen,[1] Jiabao Ju,[1] Yuanxu Gao,[1] Liujing Qu,[2,3] Yan Xia,[2,3] Yingyu Chen,[2,3,*] and Yun Bai[1,*]

[1]Department of Cell Biology, School of Basic Medical Sciences, Peking University Health Science Center, Beijing 100191, China
[2]Department of Immunology, School of Basic Medical Sciences, Peking University Health Science Center, Beijing 100191, China
[3]Peking University Center for Human Disease Genomics, Peking University, Beijing 100191, China
[4]Co-first author
*Correspondence: yingyu_chen@bjmu.edu.cn (Y.C.), baiyun@bjmu.edu.cn (Y.B.)
http://dx.doi.org/10.1016/j.stemcr.2016.01.011

SUMMARY

Self-renewal and differentiation of neural stem cells is essential for embryonic neurogenesis, which is associated with cell autophagy. However, the mechanism by which autophagy regulates neurogenesis remains undefined. Here, we show that *Eva1a/Tmem166*, an autophagy-related gene, regulates neural stem cell self-renewal and differentiation. *Eva1a* depletion impaired the generation of newborn neurons, both in vivo and in vitro. Conversely, overexpression of EVA1A enhanced newborn neuron generation and maturation. Moreover, *Eva1a* depletion activated the PIK3CA-AKT axis, leading to the activation of the mammalian target of rapamycin and the subsequent inhibition of autophagy. Furthermore, addition of methylpyruvate to the culture during neural stem cell differentiation rescued the defective embryonic neurogenesis induced by *Eva1a* depletion, suggesting that energy availability is a significant factor in embryonic neurogenesis. Collectively, these data demonstrated that EVA1A regulates embryonic neurogenesis by modulating autophagy. Our results have potential implications for understanding the pathogenesis of neurodevelopmental disorders caused by autophagy dysregulation.

INTRODUCTION

Neural stem cells (NSCs) are a class of multipotent cells responsible for generating all types of neural cells in the nervous system and for maintaining the stem cell population by self-renewal (Gage, 2000). The transition of proliferative and multipotent NSCs to fully differentiated neurons is called neurogenesis. Neurons are generated mainly from early embryonic development to early postnatal stages. After this phase, only a few neurogenic zones remain active in the adult brain (Gotz and Huttner, 2005; Ming and Song, 2011; Paridaen and Huttner, 2014). Embryonic neurogenesis is essential for the maintenance of NSCs, as well as for the generation of functional neural cell types and is therefore important for brain development and function.

Autophagy is an evolutionarily conserved process in which cellular proteins and organelles are engulfed by autophagosomes and delivered to lysosomes for degradation. Autophagy is involved in a wide variety of physiological and pathological processes, such as cancer, immune and infectious diseases, and neurodegeneration (Jaeger and Wyss-Coray, 2009; Rosello et al., 2012). Among these diseases, the role of autophagy in neurodegeneration has been studied extensively. Deletion of autophagy-related genes, such as *Atg5* and *Atg7*, caused dysregulation of autophagosome formation and consequent neurodegeneration (Komatsu et al., 2005, 2006; Kuma et al., 2004). In fact, many studies have suggested that modulators of autophagy may be used as potential therapeutic strategies to treat diseases caused by autophagy defects (Harris and Rubinsztein, 2012; Nassif and Hetz, 2011; Dalby et al., 2010). Although studies have suggested that autophagy has neuroprotective effects, the role of autophagy in regulating embryonic neurogenesis remains largely unknown.

Previous studies have demonstrated that autophagy occurs in physiological conditions in the brain during the development of the nervous system and that it plays a significant role in cell differentiation (Schweichel and Merker, 1973; Zhao et al., 2010; Zeng and Zhou, 2008). Some autophagy-related genes that function in the inhibition of neurodegeneration are also essential for CNS development. Specifically, AMBRA1, an activating molecule in BECLIN 1-regulated autophagy, is essential for the development of the nervous system (Fimia et al., 2007; Yazdankhah et al., 2014; Vazquez et al., 2012). Another autophagy-related gene, *Atg5*, plays an important role in neurogenesis and gliogenesis. (Vazquez et al., 2012; Lv et al., 2014; Wang et al., 2014). These findings suggested a critical role of autophagy in the development of the nervous system. However, the precise mechanisms through which neurogenesis is regulated by autophagy is far from being well elucidated. Many molecular targets of this process need to be identified.

EVA1A (Eva-1 homolog A), also known as TMEM166 (Transmembrane protein 166) or FAM176A (Family with sequence similarity 176), is a lysosome and ER-associated protein that can regulate cell autophagy and apoptosis (Wang et al., 2007). It is conserved in humans, chimpanzees, rats, mice, and dogs, indicating that it may have important functions in vertebrate animals. Previous studies revealed that EVA1A is expressed in a cell-type-specific and

tissue-type-specific manner and is significantly downregulated in cancer tissues (Xu et al., 2013; Sun et al., 2012; Tao et al., 2015). In vivo and in vitro experiments demonstrated that EVA1A overexpression inhibits tumor cell proliferation by autophagy (Chang et al., 2013; Xie et al., 2014). These findings suggested a close correlation between EVA1A-induced autophagy and cancer suppression. Other studies have suggested that EVA1A-induced autophagy plays a significant role in cell death following focal cerebral ischemic injury (Li et al., 2012). Lu et al. (2015) demonstrated that EVA1A/TMEM166 is a key player in C/EBPα-mediated autophagy induction and protection against starvation. However, the role of EVA1A in neurogenesis has not been reported, and the mechanism by which EVA1A regulates autophagy remains to be determined.

In the present study, we generated an *Eva1a* knockout (KO) mouse to study the physiological role of EVA1A in vivo. The analysis of *Eva1a* KO embryos and isolated NSCs revealed the function of EVA1A in self-renewal and neuronal differentiation of NSCs. Our study highlighted a previously unknown role of EVA1A in the CNS.

RESULTS

EVA1A Expression in Brain Development

To determine the role of EVA1A in brain development, we first evaluated the expression of EVA1A in the embryonic cortex from embryonic day 10.5 (E10.5) to E16.5 and postnatal 2 day (P2). Western blotting revealed that EVA1A expression increased substantially from E10.5 to E16.5 and gradually decreased after P2 (Figures S1A and S1B). Consistent with this observation, immunofluorescence and confocal microscopy observations indicated that the fluorescence signals of EVA1A were elevated at E10.5 and peaked at E16.5 (Figure S1C). Interestingly, the level of autophagy, which is indicated by the autophagy marker LC3B-II, also increased from E10.5 to E16.5 (Figures S1A, S1B, and S1D). Simultaneously, β-TUBULIN III, the neuron marker, was markedly upregulated during this period (Figures S1A, S1B, and S1E). These results demonstrate that neuron differentiation occurs at the early embryonic development stage and the initiation of neuron differentiation corresponds to the expression of EVA1A and the autophagy level, suggesting that EVA1A might be involved in brain development including neuron differentiation.

Generation of *Eva1a* Gene Knockout Mice

To investigate the physiological function of EVA1A in the development of the CNS, we generated *Eva1a* gene KO mice. To this end, we crossed *Eva1a*$^{flox/flox}$ mice (Figure 1A) with transgenic mice expressing Cre recombinase under the control of the *Nestin* promoter (*Nestin-Cre*). The *Eva1a*$^{+/+}$ and *Eva1a*$^{-/-}$ mice were identified by PCR analysis of mouse tail DNA (Figure 1B). The results of RT-PCR and western blotting demonstrated that the level of EVA1A was low or absent in the indicated brain areas (cortex, hippocampus, and cerebellum) in *Eva1a*$^{-/-}$ mice at E12.5 (Figures 1C and 1D). Consistent with this result, an immunofluorescence assay confirmed that EVA1A protein signals were nearly absent in the cortex of the *Eva1a*$^{-/-}$ mice (Figure 1E versus 1F). We also evaluated the protein level of EVA1A in other tissues, such as liver, lung, heart, and muscle. There was no significant change between the *Eva1a*$^{-/-}$ and *Eva1a*$^{+/+}$ mice (data not shown), indicating that the EVA1A deficiency was restricted to the CNS.

Eva1a Deletion Decreases the Ability of NSCs Self-Renewal, but Fails to Induce Cell Apoptosis

To investigate the role of EVA1A in NSC self-renewal, we first detected the expression of the NSCs markers, NESTIN and SOX2, in the whole-brain tissue at E12.5 in both *Eva1a*$^{-/-}$ and *Eva1a*$^{+/+}$ mice. Our results revealed that the levels of both NESTIN and SOX2 were markedly decreased in the *Eva1a*$^{-/-}$ mice (Figure 2A). We next injected bromodeoxyuridine (BrdU) into both the *Eva1a*$^{+/+}$ and *Eva1a*$^{-/-}$ mice at E12.5 and detected proliferating cells in living tissues. After 4 hr, the frozen sections were obtained from whole-brain samples and subjected to immunofluorescence assay. Confocal microscopy showed that the *Eva1a*$^{-/-}$ mice displayed a weaker signal for NESTIN staining (Figure 2B versus 2C, left panel) and the number of NESTIN^{+} BrdU^{+} positive cells was decreased in the *Eva1a*$^{-/-}$ cortex compared with those in the *Eva1a*$^{+/+}$ mice, indicating the number of newborn NSCs was reduced in the *Eva1a*$^{-/-}$ mice (Figures 2B–2D). To rule out the possibility that the reduction in NSCs was the result of cell apoptosis, we performed a terminal deoxynucleotidyl transferase dUTP nick end labeling (TUNEL) assay in brain sections. There was no significant difference in TUNEL-positive cells between *Eva1a*$^{-/-}$ and *Eva1a*$^{+/+}$ mice, indicating that the decrease in NSC self-renewal is independent of apoptosis (Figures 2E–2G).

We next investigated the influence of EVA1A on NSC self-renewal in vitro. As shown in Figures 2H and 2I, the number of secondary neurospheres generated from *Eva1a*$^{-/-}$ NSCs was markedly lower than that from *Eva1a*$^{+/+}$ NSCs. At the same time, deletion of *Eva1a* in NSCs resulted in smaller-sized neurospheres compared with their *Eva1a*$^{+/+}$ counterparts (Figures 2H and 2J), indicating defective self-renewal in *Eva1a*$^{-/-}$ NSCs. Furthermore, Annexin V staining and flow cytometry analysis indicated there was no significant difference in cell apoptosis between *Eva1a*$^{-/-}$ NSCs and *Eva1a*$^{+/+}$ NSCs (Figures 2K and 2L), excluding the possibility that the defective NSC self-renewal was

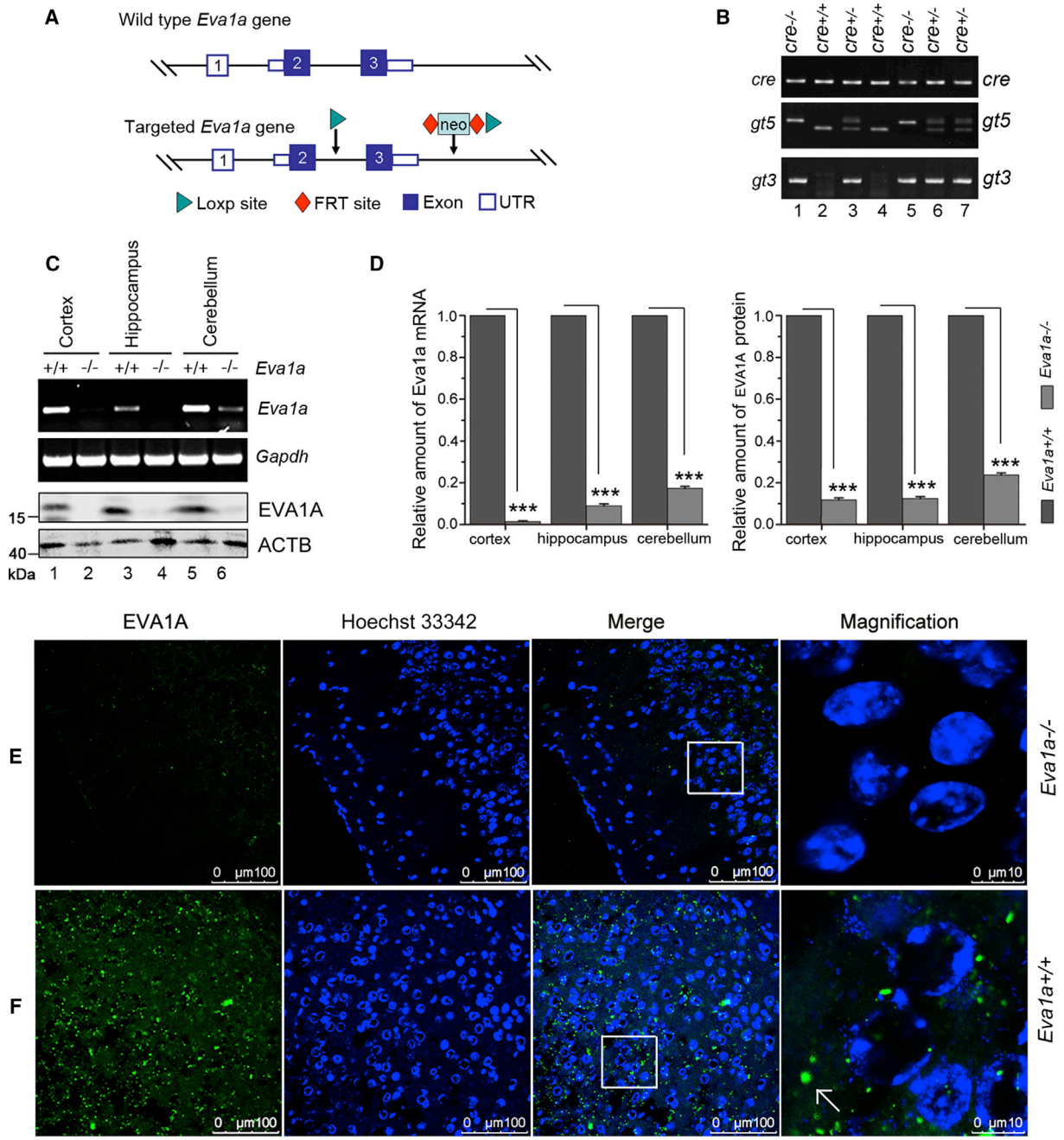

Figure 1. Generation of *Eva1a* KO Mice

(A) Scheme to generate *Eva1a* conditional knockout mice.

(B) Genomic DNA was extracted from mouse tails and analyzed by PCR.

(C) Brain homogenates (cortex, hippocampus, and cerebellum) were obtained from $Eva1a^{+/+}$ mice and $Eva1a^{-/-}$ mice at E12.5. The *Eva1a* mRNA level was analyzed by RT-PCR, and the protein level was analyzed by western blotting.

(D) Statistical analysis of the level of Eva1a in different regions of the brain. The average value in $Eva1a^{+/+}$ brain tissues was normalized as 1. Data are means ± SD of the results from three independent experiments. ***$p < 0.001$; t test.

(E and F) Frozen sections were obtained from whole-brain samples of both $Eva1a^{+/+}$ and $Eva1a^{-/-}$ mice at E12.5, and an immunofluorescence assay was carried out to detect EVA1A expression in the cortex (scale bar, 100 μm). The right panel shows higher magnifications (scale bar, 10 μm). The white arrow indicates the EVA1A protein signal in the whole-brain samples.

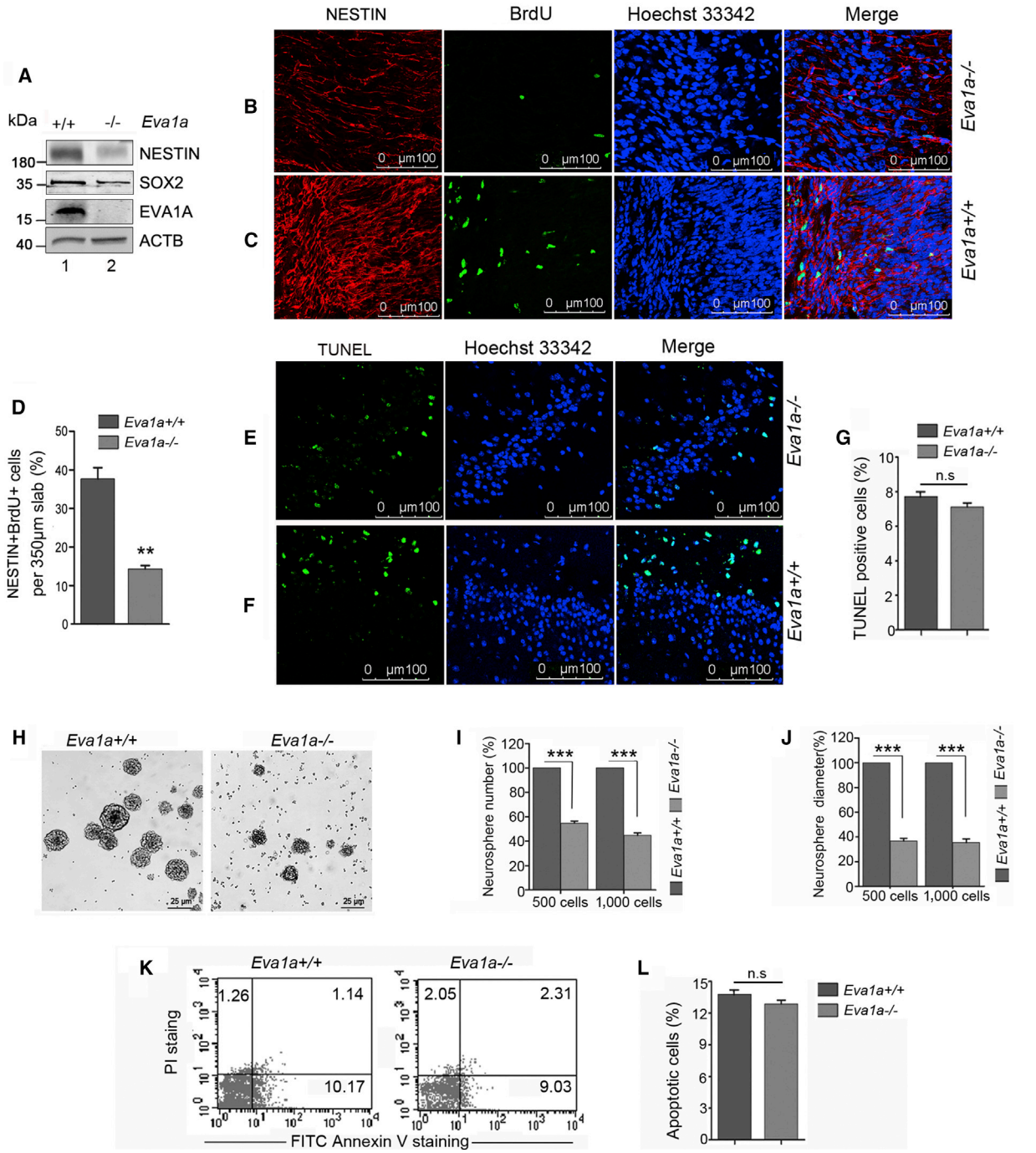

Figure 2. *Eva1a* Knockout Decreases NSCs Self-Renewal, but Fails to Induce Cell Apoptosis

(A) Immunoblot analysis of EVA1A, NESTIN, and SOX2 expressions in whole-brain tissue from *Eva1a*$^{+/+}$ and *Eva1a*$^{-/-}$ mice at E12.5.

(B and C) Pregnant female mice at E12.5 were injected intraperitoneally with BrdU 4 hr before euthanasia. Brain frozen sections were obtained and subjected to an immunofluorescence assay. Representative confocal microscopy images of the fluorescence of NESTIN and BrdU were analyzed. Scale bar, 100 μm.

(D) Quantification of BrdU and NESTIN double-positive cells within a 350-μm slab of the brain section in *Eva1a*$^{+/+}$ and *Eva1a*$^{-/-}$ littermate mice. Five randomly selected sections from each mouse were examined. Three independent experiments were performed. Data are means ± SD $^{**}p < 0.01$; t test.

(legend continued on next page)

caused by apoptosis. Collectively, these observations supported a positive role of EVA1A in NSC self-renewal.

NSCs Differentiation Is Impaired in *Eva1a*$^{-/-}$ Mice

Having demonstrated the correlation between EVA1A and NSC self-renewal, we then investigated the effect of EVA1A on NSC differentiation. We first examined the levels of both EVA1A and β-TUBULIN III (a marker of neurons) in *Eva1a*$^{-/-}$ and *Eva1a*$^{+/+}$ mice at E16.5. As shown in Figures 3A–3D, Eva1a was nearly absent in *Eva1a*$^{-/-}$, which is associated with a concomitant decrease in β-TUBULIN III protein. Data from immunofluorescence assay in brain frozen sections confirmed that the β-TUBULIN III showed a stronger fluorescence signal in *Eva1a*$^{+/+}$ mice than in *Eva1a*$^{-/-}$ mice (Figure 3E versus 3F, left panel). Meanwhile, the number of β-TUBULIN III^{+} BrdU^{+} double-positive cells within a 350-μm slab of the brain was significantly downregulated in *Eva1a*$^{-/-}$ mice (from around 31.66% to 14.33%) (Figures 3E–3G), suggesting damage to the newborn neuron population.

Next, we established NSC cultures, in which the transition from proliferative to differentiated cells can be easily monitored in short-term cell culture, following treatment with all-*trans* retinoic acid for direct neuronal differentiation. NSCs from *Eva1a*$^{+/+}$ and *Eva1a*$^{-/-}$ mice at E12.5 were cultured under differentiation conditions for 6 days. The levels of β-TUBULIN III were lower in *Eva1a*$^{-/-}$ NSC cultures (Figures 3H and 3I). Consistent with the results of western blotting, the percentage of β-TUBULIN III^{+} differentiated neurons was decreased in *Eva1a*$^{-/-}$ NSC cultures (Figures 3J and 3K). We also found that the neurites of *Eva1a*$^{-/-}$ neurons were shorter than those from *Eva1a*$^{+/+}$ neurons (Figures 3J and 3L), indicating a deficiency in neurite formation and neuron maturation. Collectively, these data suggested that EVA1A may be important for the neuronal differentiation of NSCs.

EVA1A Modulates Autophagy through the PIK3CA/AKT-mTOR Pathway

Previous studies have demonstrated that dysregulation of autophagy can lead to abnormal neuronal hyperproliferation, cell death, and differentiation (Levine and Kroemer, 2008; Cecconi et al., 2007). We observed that autophagy is activated during embryonic neurogenesis, which is accompanied by an increase in EVA1A levels (Figure S1). Therefore, we hypothesized that EVA1A might regulate embryonic neurogenesis via autophagy. Initially, we analyzed the autophagy-related genes in the cortex of both *Eva1a*$^{+/+}$ and *Eva1a*$^{-/-}$ mice at E16.5. We found that the mRNA levels of *Atg5* and *Lc3b* were decreased in *Eva1a*-depleted cortex tissue (Figure 4A). We next measured the conversion of LC3B using western blotting. The conversion of LC3B-I to LC3B-II occurs during autophagy, and the amount of LC3B-II is correlated with the number of autophagosomes (Klionsky et al., 2012). It was shown that the accumulation of LC3B-II was reduced in the *Eva1a*$^{-/-}$ cortex compared with the *Eva1a*$^{+/+}$ cortex (Figure 4B). Consistent with the results of western blotting, confocal microscopy observation indicated that the number of LC3B puncta was decreased in the *Eva1a*$^{-/-}$ cortex (Figure 4C versus 4D).

It has been widely recognized that the SQSTM1 (sequestosome 1)/P62 protein serves as a link between LC3 and ubiquitinated substrates. It incorporates into the completed autophagosome and is degraded in lysosome. Therefore, the level of SQSTM1 is a marker for autophagic flux (Klionsky et al., 2012). As shown in Figure 4B, the basal level of SQSTM1 was upregulated and formed numerous aggregates in the *Eva1a*$^{-/-}$ cortex compared with the *Eva1a*$^{+/+}$ cortex (Figure 4E versus 4F). The presence of strong ubiquitin staining was also observed in the *Eva1a*$^{-/-}$ cortex (Figure 4G versus 4H), indicating blockage of autophagic flux.

In vitro experiments were next performed to corroborate the above-mentioned autophagic phenotypes. NSCs were generated from both *Eva1a*$^{-/-}$ and *Eva1a*$^{+/+}$ mice at E12.5. RT-PCR showed that loss of *Eva1a* in NSCs resulted in a reduction of *Atg5* and *Lc3b* mRNA levels (Figure 5A). Simultaneously, decreased LC3B-II and increased SQSTM1 protein levels were also observed in *Eva1a*$^{-/-}$ NSCs compared with *Eva1a*$^{+/+}$ NSCs (Figure 5B). Consistent with the results of western blotting, the number of LC3B dots per cell in *Eva1a*$^{-/-}$ NSCs was significantly decreased

(E and F) Frozen sections were obtained from whole-brain samples of both *Eva1a*$^{+/+}$ and *Eva1a*$^{-/-}$ mice at E12.5, and subjected to a TUNEL assay. Representative confocal microscopy images of the fluorescence were analyzed. Scale bar, 100 μm.
(G) The percentage of TUNEL-positive cells was calculated as the mean of ten different fields from each section. Five randomly selected sections from each mouse were examined. Three independent experiments were performed. Data are means ± SD. n.s., not significant.
(H) *Eva1a*$^{+/+}$ and *Eva1a*$^{-/-}$ NSCs were grown from E12.5 embryos under proliferative conditions. Neurosphere formation was viewed under phase contrast microscopy and representative microscopy images are shown. Scale bar, 25 μm.
(I and J) *Eva1a*$^{+/+}$ and *Eva1a*$^{-/-}$ NSCs were cultured in 96-well non-coated plates with 500 or 1,000 cells per well under the same conditions as in (H). The relative neurosphere number and diameter were calculated as shown in the histograms. The average value in the *Eva1a*$^{+/+}$ group was normalized as 100%. Data are means ± SD of the results from three independent experiments. ***$p < 0.001$; t test.
(K) *Eva1a*$^{+/+}$ and *Eva1a*$^{-/-}$ NSCs were grown from E12.5 embryos under proliferative conditions. Cell apoptosis was detected using the FITC-Annexin V plus propidium iodide staining kit by flow cytometry.
(L) Apoptotic cells were calculated and each bar represents the mean ± SD from three independent experiments. n.s., not significant.

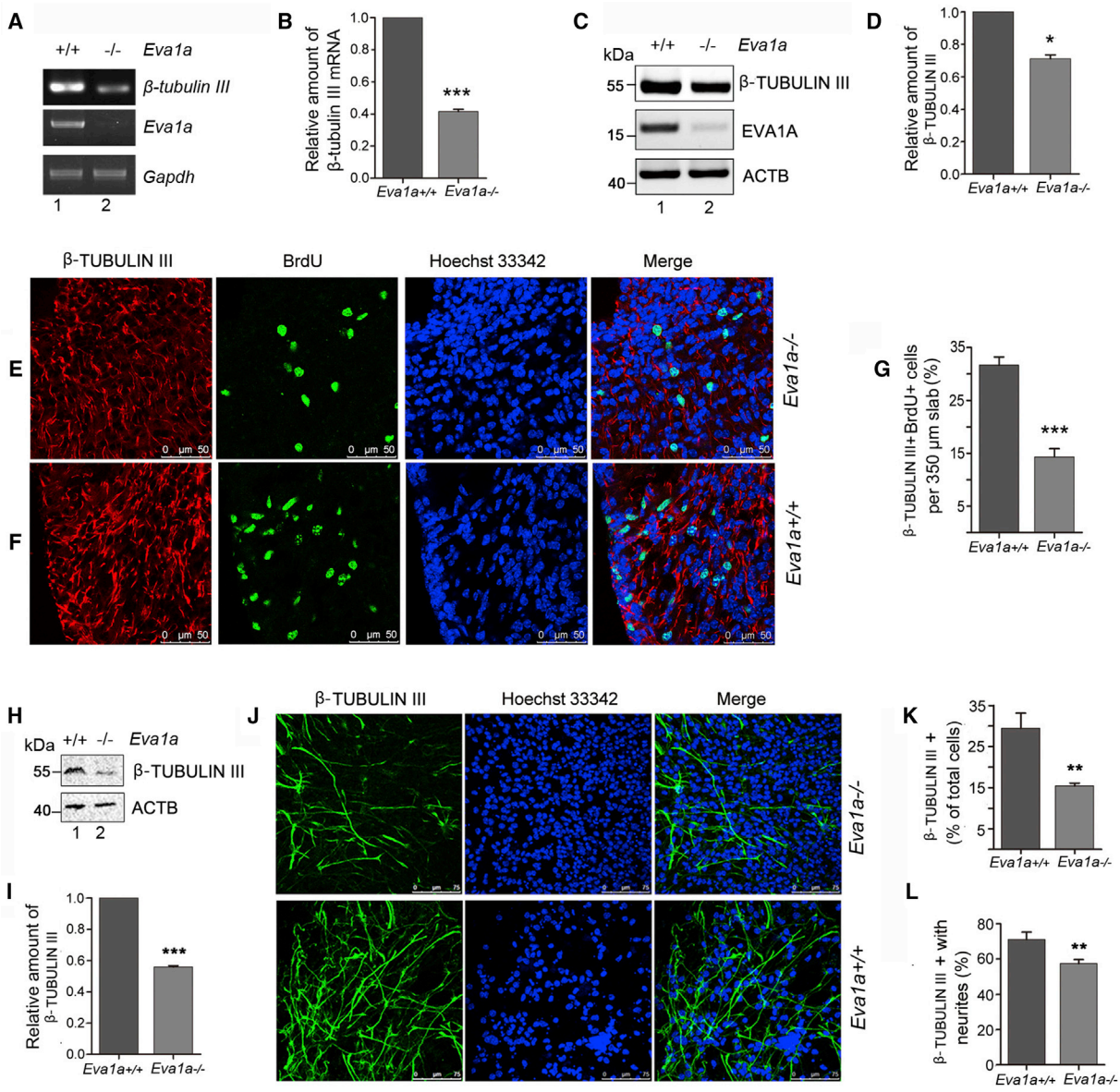

Figure 3. NSC Differentiation Is Impaired in *Eva1a* KO Mice

(A) RT-PCR analysis of *Eva1a* and *β-tubulin III* mRNA in whole-brain tissue from $Eva1a^{+/+}$ and $Eva1a^{-/-}$ mice at E16.5.

(B) Quantifications of the ratio of *β-tubulin III/Gapdh*. The average value in the $Eva1a^{+/+}$ group was normalized as 1. Data are means ± SD of the results from three independent experiments. ***$p < 0.001$; t test.

(C) Immunoblot analysis of EVA1A and β-TUBULIN III expression in whole-brain tissue from $Eva1a^{+/+}$ and $Eva1a^{-/-}$ mice at E16.5.

(D) Histogram shows the ratio of β-TUBULIN III/ACTB. The average value in the $Eva1a^{+/+}$ group was normalized as 1. Data are means ± SD of the results from three independent experiments. *$p < 0.05$; t test.

(E and F) Pregnant female mice at E16.5 were injected intraperitoneally with BrdU 4 hr before euthanasia. Brain frozen sections were obtained and subjected to an immunofluorescence assay. Representative confocal microscopy images of the fluorescence of β-TUBULIN III and BrdU were analyzed. Scale bar, 50 μm.

(G) Quantification of β-TUBULIN III and BrdU double-positive cells within a 350-μm slab of the brain section in $Eva1a^{+/+}$ and $Eva1a^{-/-}$ littermate mice. Five randomly selected sections from each mouse were examined. Three independent experiments were performed. Data are means ± SD ***$p < 0.001$; t test.

(H) NSCs from $Eva1a^{+/+}$ and $Eva1a^{-/-}$ mice at E12.5 were cultured under differentiation conditions for 6 days. The levels of β-TUBULIN III were evaluated by western blotting.

(legend continued on next page)

compared with that in *Eva1a*$^{+/+}$ NSCs (Figures 5C and 5D). These data were consistent with those from the mouse cortex. Taken together, our data suggested that autophagic activity was impaired in *Eva1a*$^{-/-}$ cells. Importantly, the decrease of β-TUBULIN III levels in the *Eva1a*$^{-/-}$ cortex was associated with decreased LC3B puncta, as well as increased SQSTM1 accumulation (Figures 4C–4F), indicating that *Eva1a* depletion-triggered damage to neurogenesis might result from disrupted autophagy.

We then investigated the mechanisms of the autophagy defective in *Eva1a*$^{-/-}$ cells. The mammalian target of rapamycin (mTOR) has been known as a negative regulator of autophagy. Experiments showed that the phosphorylation levels of mTOR at Ser2448 (activation site) and RPS6KB1 (ribosomal protein S6 kinases, 70 kDa, polypeptide 1, a substrate of mTOR) as well as EIF4EBP1 (Eukaryotic translation initiation factor 4E binding protein 1), two downstream effectors of mTOR, were elevated in the *Eva1a*$^{-/-}$ cortex (Figures 4I and 4J). Furthermore, we examined mTOR signaling in NSCs from both *Eva1a*$^{-/-}$ and *Eva1a*$^{+/+}$ NSCs at E12.5. As shown in Figures 5E and 5F, the levels of p-mTOR, p-RPS6KB1, and p-EIF4EBP1 were elevated in the *Eva1a*$^{-/-}$ NSCs. Collectively, these results support the hypothesis that an increase of mTOR activity contributes functionally to the autophagy defect in *Eva1a*$^{-/-}$ cells.

The PIK3CA-AKT signaling pathway plays a key role in various cellular processes, including cell growth, proliferation, survival, and autophagy. Activation of PIK3CA results in phosphorylation of phosphatidylinositol 4,5-bisphosphate (PIP2) to form PIP3. Subsequently, PIP3 recruits downstream effector proteins such as serine/threonine kinase AKT. Once activated, AKT-mediated phosphorylation of TSC2 (tuberous sclerosis complex 2) inhibits the TSC1-TSC2 complex function, and thus activates mTOR signaling. Therefore, further experiments were performed to determine the influence of *Eva1a* deletion on PIK3CA-AKT signal. As shown in Figures 4K and 4L, there was a significant increase in the phosphorylation of PIK3CA and AKT in the *Eva1a*$^{-/-}$ cortex at E16.5. Importantly, the basal phosphorylation levels of TSC2 were decreased. Similarly, we analyzed the PIK3CA/AKT signaling pathway in NSCs at E12.5. Consistent results were obtained in the absence of *Eva1a* in NSCs (Figures 5G and 5H). Taken together, these results suggested that loss of *Eva1a* leads to the activation of the PIK3CA-AKT axis, which results in the inactivation of TSC2 and the subsequent activation of mTOR signals.

Overexpression of EVA1A Restores Self-Renewal and Neuronal Differentiation in *Eva1a*$^{-/-}$ NSCs

Eva1a depletion induced defects in NSC differentiation; therefore, we performed reciprocal EVA1A gain-of-function experiments using NSCs at E12.5 and an *Ad5-Eva1a* construct. The number and the size (diameter) of secondary neurosphere formed from the NSCs were used as a measure of NSC self-renewal. Our results showed that neurosphere formation was decreased in *Eva1a*-deleted NSCs compared with that of *Eva1a*$^{+/+}$ NSCs. However, overexpression of EVA1A in *Eva1a*$^{-/-}$ NSCs increased the number of neurospheres (Figures 6A and 6B, left panel). Meanwhile, the neurosphere diameter in EVA1A-overexpressing *Eva1a*$^{-/-}$ NSCs was greater than that of *Eva1a*$^{-/-}$ NSCs alone (Figures 6A and 6B, right panel). In addition, *Eva1a*$^{-/-}$ NSCs allowed to differentiate in cultures generated a small number of β-TUBULIN III-positive neurons compared with that in *Eva1a*$^{+/+}$ NSCs (Figure 6D, left panel). After EVA1A overexpression in *Eva1a*$^{-/-}$ NSCs, the percentage of differentiated neurons increased from around 15% to 25% (Figure 6D, left panel). Furthermore, compared with the *Eva1a*$^{-/-}$ NSCs alone, the *Eva1a*$^{-/-}$ NSCs overexpressing EVA1A appeared to produce longer neurites (Figures 6C and 6D, right panel), indicating enhanced neuronal differentiation and maturation by EVA1A overexpression. These results suggested that *Eva1a* depletion-induced deficiency in neurogenesis can be rescued by overexpression of EVA1A, indicating the specificity of EVA1A function.

Eva1a depletion leads to the activation of the PIK3CA/AKT-mTOR pathway; therefore, we examined whether overexpression of EVA1A could inactivate this pathway and increase autophagy levels. As expected, overexpression of EVA1A in *Eva1a*$^{-/-}$ NSCs enhanced the conversion of LC3B and SQSTM1 degradation (Figures 6E and 6F, lane 3 versus lane 2), suggesting the activation of autophagy. Simultaneously, overexpression of EVA1A in *Eva1a*$^{-/-}$ NSCs significantly downregulated the levels of p-RPS6KB1 and p-EIF4EBP1 (Figures 6E and 6F, lane 3 versus lane 2), indicating the inhibition of the mTOR signal. We subsequently detected the PIK3CA-AKT signal in such conditions. As shown in Figures 6G and 6H, the phosphorylation

(I) Quantifications of the amount β-TUBULIN III protein relative to ACTB are shown. The average value in the *Eva1a*$^{+/+}$ group was normalized as 1. Data are means ± SD of the results from three independent experiments. ***$p < 0.001$; t test.

(J) The treatment of NSCs was the same as in (H), after which, the cells were subjected to immunostaining against β-TUBULIN III and viewed under a confocal microscope. Scale bar, 75 μm.

(K and L) Five randomly selected areas from each slide were examined for the percentage of β-TUBULIN III^{+}-differentiated neurons and β-TUBULIN III^{+} cells with neurites under the fluorescence microscope. Three independent experiments were performed. Data are means ± SD. **$p < 0.01$; t test.

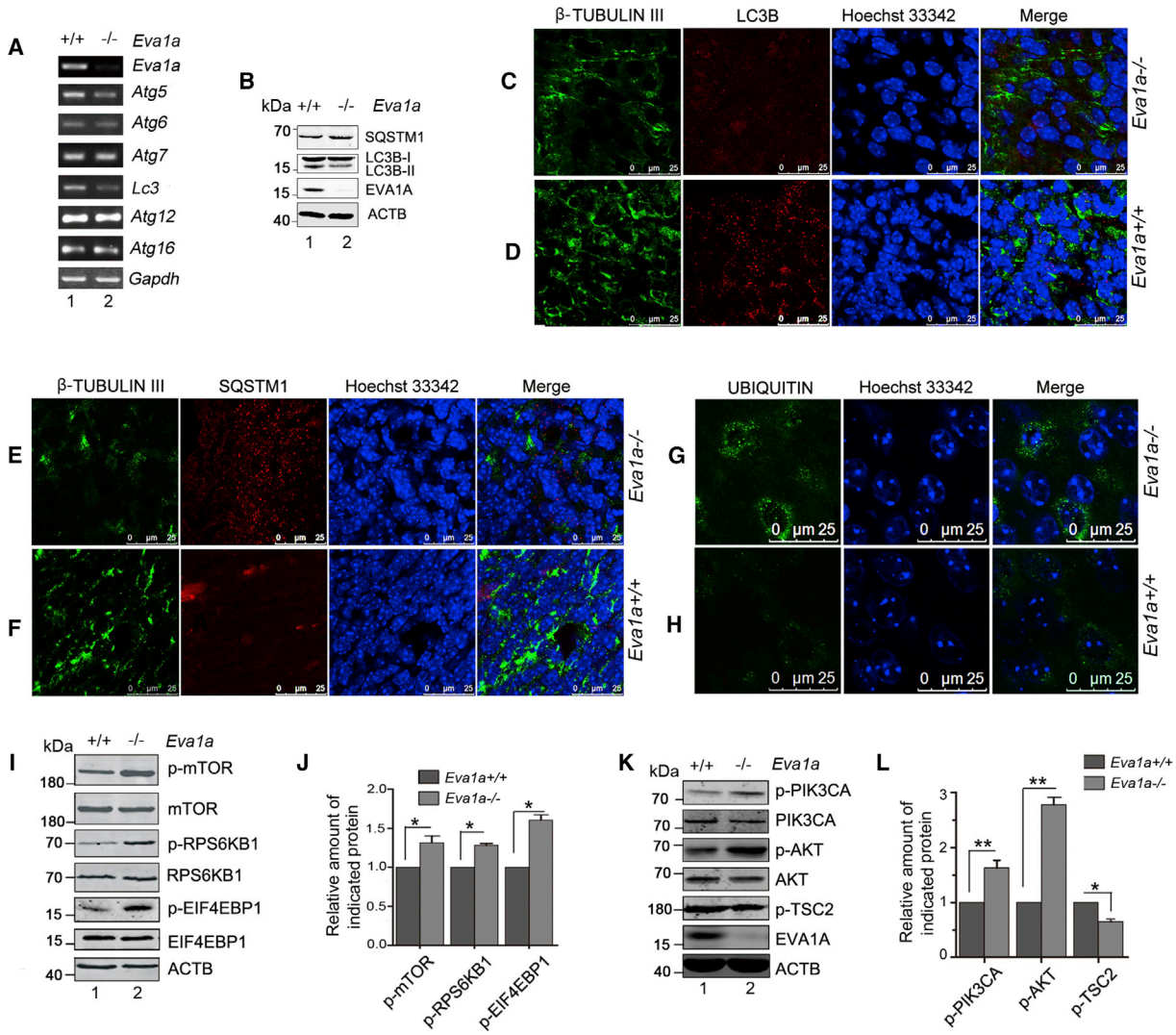

Figure 4. EVA1A Modulates Autophagy through the PIK3CA/AKT-mTOR Pathway

(A) The mRNA levels of autophagy-related genes in whole-brain tissue from *Eva1a*$^{+/+}$ and *Eva1a*$^{-/-}$ mice at E16.5 were detected by RT-PCR.

(B) The protein levels of SQSTM1 and LC3B in whole-brain tissue were detected by western blotting.

(C–F) Brain frozen sections were obtained from both *Eva1a*$^{+/+}$ and *Eva1a*$^{-/-}$ mice at E16.5, which were then subjected to an immunofluorescence assay. Representative confocal microscopy images of the distribution of β-TUBULIN III, LC3B, and SQSTM1 were analyzed.

(G and H) Representative confocal microscopy images of the distribution of ubiquitin are shown. Scale bar, 25 μm.

(I and K) Western blot analysis with the indicated antibodies in whole-brain tissue from both *Eva1a*$^{+/+}$ and *Eva1a*$^{-/-}$ mice at E16.5.

(J and L) Densitometric analysis of the immunoblots. ACTB was assessed as a loading control. The average value in the *Eva1a*$^{+/+}$ group was normalized as 1. Data are means ± SD of the results from three independent experiments. **p* < 0.05, ***p* < 0.01; t test.

levels of PIK3CA and AKT were decreased and TSC2 phosphorylation was increased in *Eva1a*$^{-/-}$ NSCs overexpressed by Eva1a. Furthermore, a PIK3CA/AKT inhibitor (perifosine) was used to confirm the relationship between EVA1A-regulated autophagy and the PIK3CA/AKT-mTOR pathway. Data from experiments indicated that perifosine-mediated inhibition of PIK3CA/AKT-mTOR at least partly rescued autophagy deficiency in *Eva1a*$^{-/-}$ NSCs at E16.5 (Figures S2A–S2D). Importantly, we observed that perifosine treatment could partly reverse the defective self-renewal and defective differentiation caused by *Eva1a* knockout (Figures S2E–S2H). These data further confirmed that EVA1A regulates autophagy via the suppression of the PIK3CA/AKT-mTOR signaling, and that EVA1A-mediated autophagy is involved in self-renewal and neuronal differentiation.

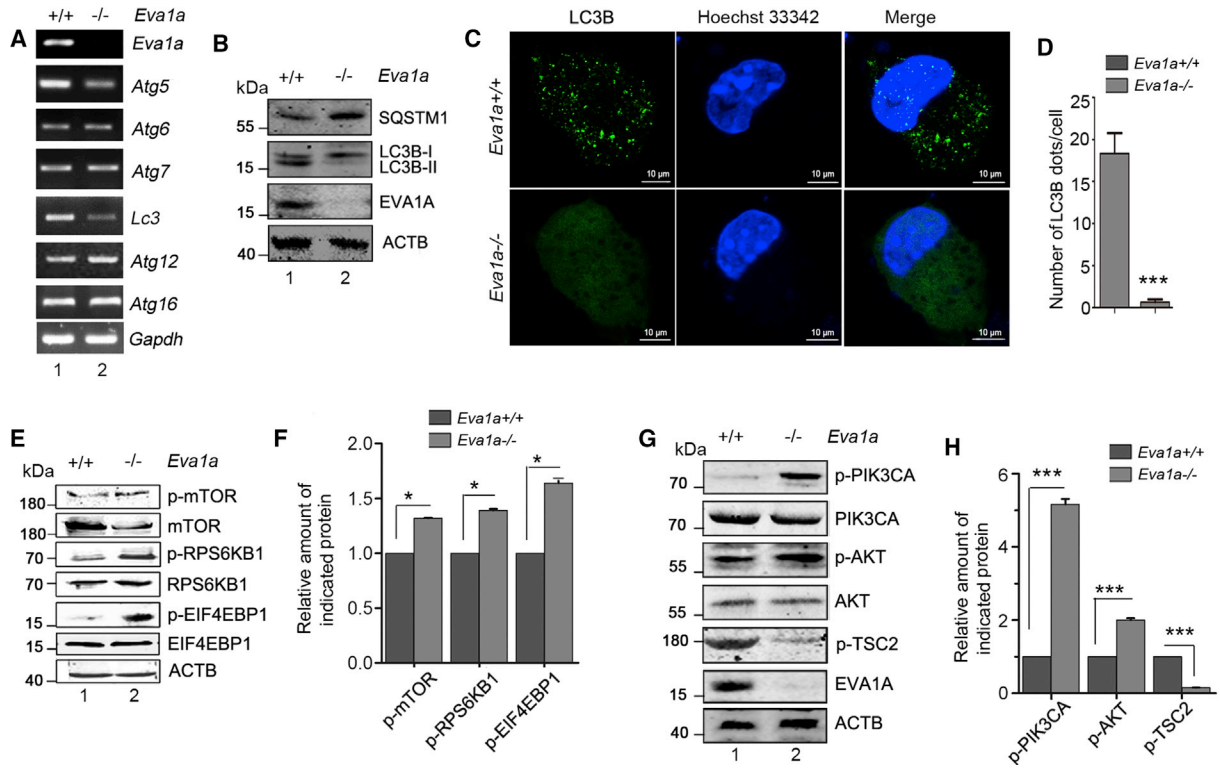

Figure 5. *Eva1a* Knockout in NSCs Increases the PIK3CA/AKT-mTOR Signal Pathway

(A) NSCs from *Eva1a*$^{+/+}$ and *Eva1a*$^{-/-}$ at E12.5 were cultured under proliferation conditions. The mRNA levels of autophagy-related genes were detected by RT-PCR.

(B) The treatment of NSCs was the same as in (A). The levels of LC3B and SQSTM1 were analyzed by western blotting.

(C) The treatment of NSCs was the same as in (A). The cells were then plated on glass coverslips coated with poly-ornithine for 24 hr. NSCs were subjected to immunofluorescence against LC3B and viewed under a confocal fluorescence microscopy. Scale bar, 10 μm.

(D) Histogram showing the quantification of the numbers of LC3B puncta per cell under confocal microscopy. Three independent experiments were performed. Results are means ± SD of at least 100 non-overlapping cells scored. ***$p < 0.01$; t test.

(E and G) The treatment of NSCs was the same as in (A). NSCs were lysed and subjected to immunoblot analysis using the indicated antibodies.

(F and H) Densitometric analysis of the immunoblots. ACTB was assessed as a loading control. The average value in the *Eva1a*$^{+/+}$ group was normalized as 1. Data are means ± SD of the results from three independent experiments. *$p < 0.05$, ***$p < 0.001$; t test.

Eva1a Depletion Induced Impaired NSC Differentiation Can Be Reversed by Methylpyruvate and Rapamycin

Autophagy is a potential energy source during cellular restructuring, which is associated with neuronal differentiation and neurite outgrowth (Hara et al., 2006; Levine and Klionsky, 2004). A recent study has demonstrated that autophagy inhibition with 3-methyladenine (3-MA) reduces ATP levels during retinal neurogenesis, and this inhibition could be reversed by treatment with methylpyruvate (MP) (Mellen et al., 2008). MP is a permeable analog for the citric acid cycle. To clarify the correlation among EVA1A, neurogenesis, and the availability of energy in the course of autophagy, we performed the following test. NSCs from *Eva1a*$^{+/+}$ and *Eva1a*$^{-/-}$ mice at E12.5 were grown as neurospheres and cultured under differentiation conditions for 6 days. In the *Eva1a*$^{-/-}$ group, the number of β-TUBULIN III^{+} neurons was decreased (Figures 7A, 7B, and 7E), and the neurite length appeared shorter than that from the *Eva1a*$^{+/+}$ NSC group in the normal culture (Figures 7A, 7B, and 7F), which indicated a decrease in neuronal differentiation. However, MP treatment markedly increased the number of β-TUBULIN III^{+} neurons and the neurite length in the *Eva1a*$^{-/-}$ group (Figures 7C–7F), while no significant changes were observed in the *Eva1a*$^{+/+}$ group with or without MP treatment (Figures 7A and 7C). Simultaneously, we further detected the autophagy levels under such conditions. In normal culture conditions, the expression of β-TUBULIN III protein was downregulated in *Eva1a*$^{-/-}$ NSCs

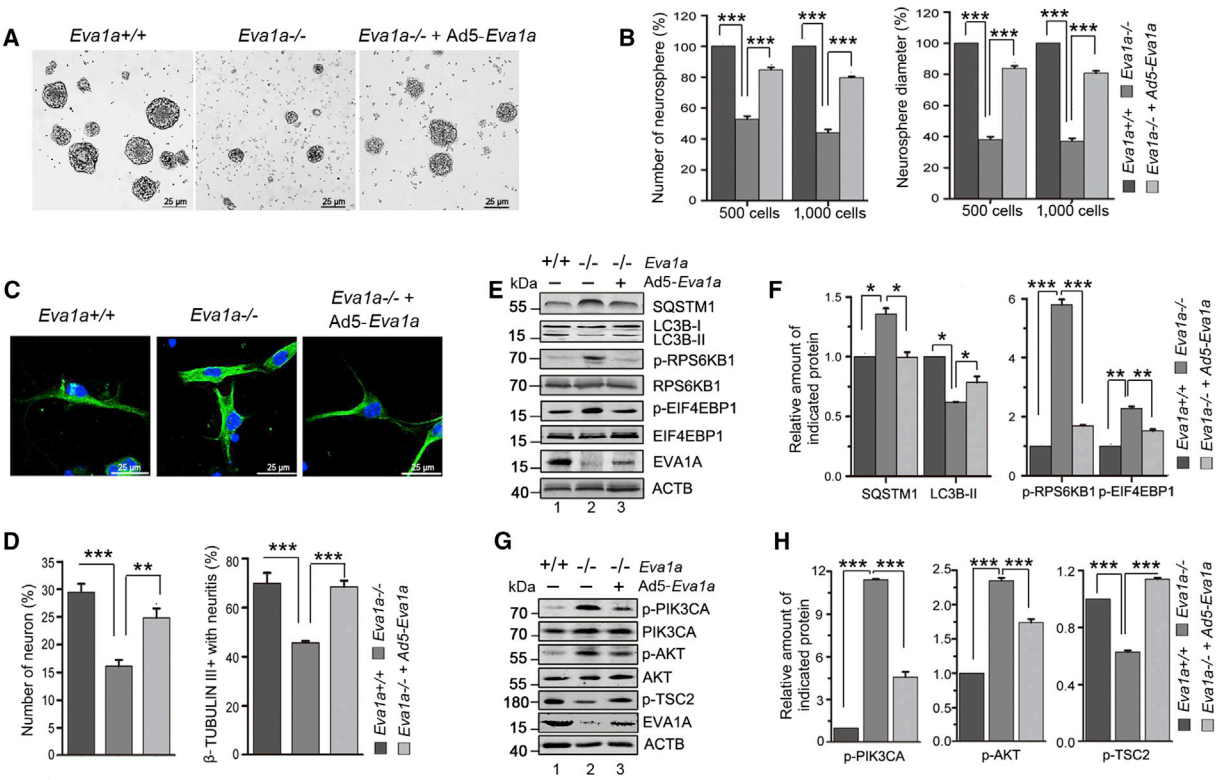

Figure 6. Overexpression of EVA1A Restores Self-Renewal and Neuronal Differentiation in *Eva1a*$^{-/-}$ NSCs

(A) NSCs obtained from *Eva1a*$^{+/+}$ and *Eva1a*$^{-/-}$ at E12.5 were infected or not infected with *Ad5-Eva1a* and further cultured for 12 hr under proliferative conditions. Neurosphere formation in NSCs from *Eva1a*$^{+/+}$, *Eva1a*$^{-/-}$ and *Eva1a*$^{-/-}$ plus *Ad5-Eva1a* were viewed by phase contrast optical microscopy. Scale bar, 25 μm.

(B) NSCs from *Eva1a*$^{+/+}$ and *Eva1a*$^{-/-}$ mice were cultured in 96-well non-coated plates with 500 or 1,000 cells per well under the same conditions as in (A). The number and the size (diameter) of secondary neurospheres were evaluated. The average value in the *Eva1a*$^{+/+}$ group was normalized as 100%. Data are means ± SD of the results from three independent experiments. ***$p < 0.001$; one-way ANOVA with Tukey's post hoc test.

(C) NSCs obtained from *Eva1a*$^{+/+}$ and *Eva1a*$^{-/-}$ at E12.5 were infected or not infected with *Ad5-Eva1a* and cultured under differentiation conditions for 6 days. Then the cells were subjected to immunostaining against β-TUBULIN III and viewed under a fluorescence microscope.

(D) Five randomly selected areas from each slide were examined for the percentage of β-TUBULIN III^{+}-differentiated neurons in total cells and β-TUBULIN III^{+} cells with neurites under the fluorescence microscope. Three independent experiments were performed. Data are means ± SD. **$p < 0.01$, ***$p < 0.001$; one-way ANOVA with Tukey's post hoc test.

(E and G) The treatment of NSCs was the same as in (A). NSCs were lysed and subjected to immunoblot analysis using the indicated antibodies.

(F and H) Densitometric analysis of the immunoblots. ACTB was assessed as a loading control. The average value in the *Eva1a*$^{+/+}$ group was normalized as 1. Data are means ± SD of the results from three independent experiments. *$p < 0.05$, **$p < 0.01$, ***$p < 0.001$; one-way ANOVA with Tukey's post hoc test.

compared with that of *Eva1a*$^{+/+}$ NSCs (Figures 7G and 7H, lane 3 versus lane 1). Meanwhile, decreased β-TUBULIN III was accompanied by weakened LC3B-II accumulation and increased SQSTM1 levels (Figures 7G and 7H, lane 3 versus lane 1), which was consistent with the above observation. After treatment with MP, β-TUBULIN III expression showed weak upregulation. At the same time, accumulation of LC3B-II was significantly elevated and a decrease in SQSTM1 levels was observed in *Eva1a*$^{-/-}$ NSCs (Figures 7G and 7H, lane 4 versus lane 3). Data from transmission electron microscopy analysis shown that MP treatment increased autophagic structures in the *Eva1a*$^{-/-}$ NSCs compared with that in *Eva1a*$^{-/-}$ NSCs alone (Figure S3), suggesting enhanced autophagy. Collectively, these results implied that MP treatment recovers impaired autophagy in *Eva1a*$^{-/-}$ NSCs.

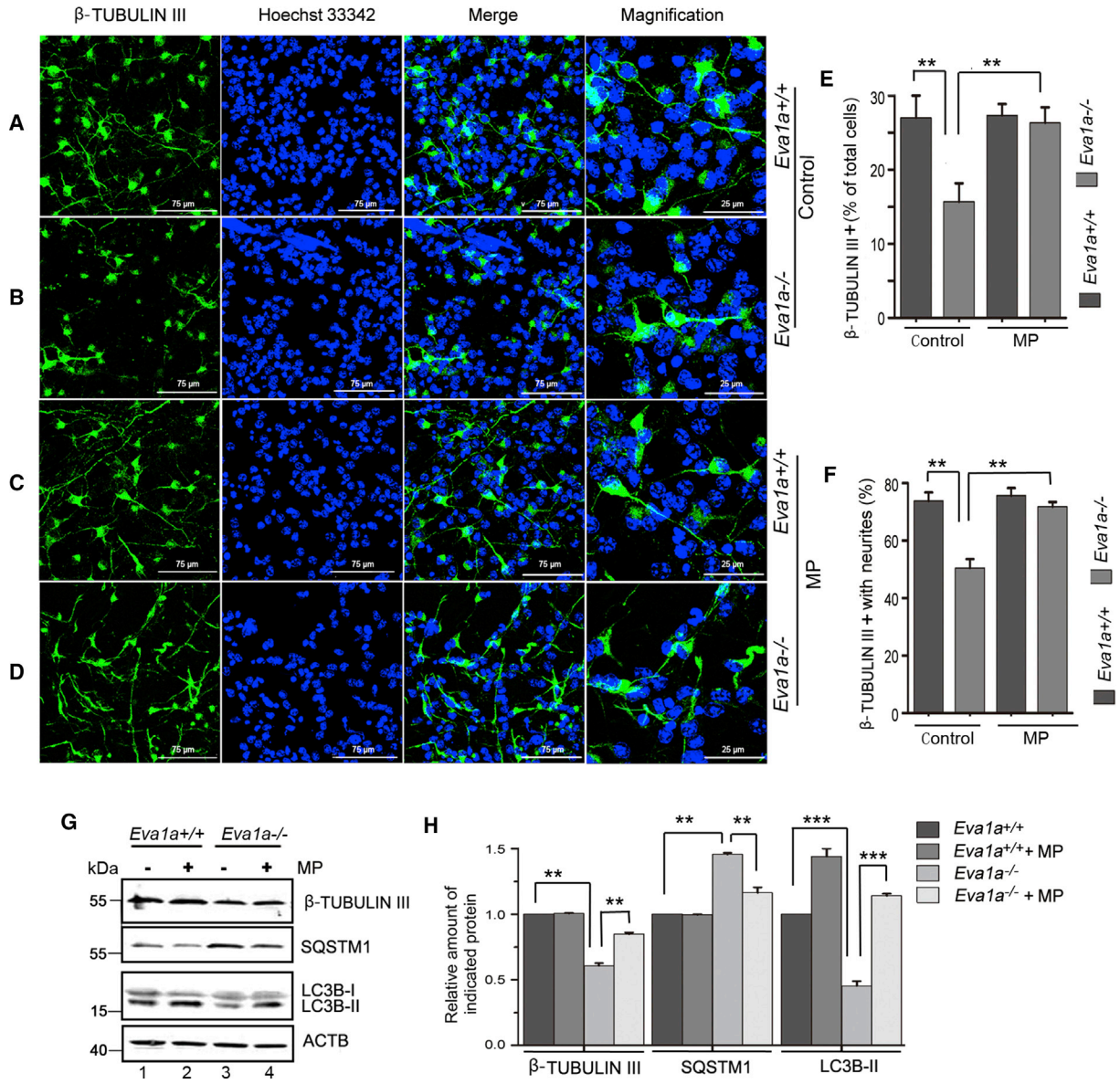

Figure 7. MP Treatment Rescues NSC Differentiation in *Eva1a*$^{-/-}$ Mice

(A–D) NSCs from *Eva1a*$^{+/+}$ and *Eva1a*$^{-/-}$ at E12.5 were grown as neurospheres, and then plated under differentiation conditions for 6 days with or without MP (10 mM) treatment. Cells were fixed for immunofluorescence analysis. Representative fields of *Eva1a*$^{+/+}$ and *Eva1a*$^{-/-}$ neurons were stained with β-TUBULIN III antibodies. Nuclei were stained with Hoechst 33342 (scale bar, 75 μm). The right panel shows higher magnifications (scale bar, 25 μm).

(E and F) Five randomly selected areas from each slide were examined for the percentage of β-TUBULIN III^{+}-differentiated neurons in total cells and β-TUBULIN III^{+} cells with neurites under the fluorescence microscope. Three independent experiments were performed. Data are means ± SD. $^{**}p < 0.01$; one-way ANOVA with Tukey's post hoc test.

(G) The treatment of NSCs was the same as in (A–D), after which the NSCs were lysed and subjected to immunoblot analysis using the indicated antibodies.

(H) Histogram showing the quantification of the ratio of the relative proteins/ACTB. The average value in the *Eva1a*$^{+/+}$ group (lane 1) was normalized as 1. Data are means ± SD of the results from three independent experiments. $^{**}p < 0.01$, $^{***}p < 0.001$; one-way ANOVA with Tukey's post hoc test.

To further consolidate the hypothesis that defective neurogenesis is caused by autophagy deficiency, we utilized the mTOR-dependent chemical rapamycin and mTOR-independent chemical lithium (LiCl) to induce autophagy for the rescue assay. As shown in Figures S4A and S4B, rapamycin could increase autophagy both in *Eva1a*$^{+/+}$ and *Eva1a*$^{-/-}$ NSCs at E16.5. LiCl treatment could enhance autophagy in *Eva1a*$^{+/+}$ NSCs (Figures S4C and S4D, lane 2 versus lane 1), but failed in *Eva1a*$^{-/-}$ NSCs (Figures S4C and S4D, lane 4 versus lane 3), indicating that the autophagy impairment caused by *Eva1a* deletion is associated with the mTOR activity.

We further examined the differentiation of NSCs under the same treatment conditions. Data obtained from western blotting indicated that rapamycin treatment could increase the levels of β-TUBULIN III in *Eva1a*$^{-/-}$ NSCs (Figures S4A and S4B, lane 4 versus lane 3). LiCl, however, had no effect on the level of β-TUBULIN III in *Eva1a*$^{-/-}$ NSCs (Figures S4C and S4D, lane 4 versus lane3). Simultaneously, we found that rapamycin treatment, but not LiCl, enhanced the formation and maturation of neurons in *Eva1a*$^{-/-}$ NSCs (Figures S4E–S4H). Together, our data reveal that the defective neurogenesis in *Eva1a*$^{-/-}$ NSCs could be rescued by mTOR-dependent autophagy modulators, at least partly.

DISCUSSION

In the present study, the role of EVA1A/TMEM166 in the process of neurogenesis was investigated using *Eva1a* KO mice. We demonstrated that EVA1A regulates NSC self-renewal and neuronal differentiation by modulating autophagy. Genetic disruption of *Eva1a* caused a deficiency in the autophagic machinery, which consequently impaired the differentiation process, decreasing the number of newborn neurons and impeding their maturation in culture. This effect could be rescued by overexpression of EVA1A or treatment with MP in vitro. Our studies suggest strongly that EVA1A modulates the process of autophagy, which may provide energy for the transition from NSCs to mature neurons.

Several studies have suggested that autophagy is activated during nervous system development and cell differentiation (Nassif and Hetz, 2011; Schweichel and Merker, 1973; Zhao et al., 2010). Initially, we observed that the EVA1A levels increased over the course of neurogenesis, along with a concomitant increase in autophagy in wild-type mice. Based on this, we speculated that increased expression of EVA1A in NSCs may play a role in neurogenesis. Here, we present several lines of evidence that demonstrate that the loss of EVA1A leads to substantial decline in NSC self-renewal, as well as in neuronal differentiation in vivo and in vitro. The phenotype changes observed in *Eva1a*-deleted NSCs could be rescued by a gain-of-function assay in vitro.

The mechanism by which EVA1A regulates neurogenesis is unclear. Autophagy plays a critical role in neurogenesis and is mainly regulated by the mTOR pathway; therefore, we examined the effect of *Eva1a* depletion on the mTOR pathway. The phosphorylation levels of mTOR, RPS6KB1, and EIF4EBP1 were increased in NSCs derived from *Eva1a*$^{-/-}$ mice. Consistent with these findings, the levels of p-PIK3CA and p-AKT (upstream of mTOR) also increased in *Eva1a*-depleted cells, which was accompanied by a substantial decrease in p-TSC2 levels. Thus, it can be seen that the PIK3CA-AKT signal negatively regulates TSC1/2 and activates mTOR, and consequently, inhibits autophagy. Importantly, transduction of *Ad5-Eva1a* in *Eva1a*$^{-/-}$ NSCs attenuated this PIK3CA/AKT-mTOR signaling pathway, and restored the autophagy level. These results were consistent with those of a previous report, which indicated that overexpression of EVA1A/TMEM166 decreased the activity of mTOR in human tumor cells (Chang et al., 2013). Our studies indicated that EVA1A probably regulates neurogenesis through the PIK3CA/AKT-mTOR pathway. However, further studies are necessary to understand how EVA1A regulates the PIK3CA/AKT axis precisely.

Autophagy is a complex catabolic program that functions in the lysosomal degradation of proteins and other subcellular constituents and serves as an effective method of providing metabolic precursors. Previous studies demonstrated that neuroepithelial cells undergo differentiation in an energy-consuming process (Vazquez et al., 2012; Mellen et al., 2008; Qu et al., 2007), and autophagy can provide sufficient energy for the process of neurogenesis. Until recently, only a few studies had demonstrated the effects of autophagy on neurogenesis in vivo. However, how autophagy regulates neurogenesis remains largely unknown. In this study, we observed that NSC self-renewal and differentiation were decreased in *Eva1a*-deficient mice and autophagy was decreased. Decreased levels of autophagy may lead to a shortage of energy supply and impede the process of neurogenesis; therefore, we treated *Eva1a*-defective NSCs with MP. Generally, MP treatment restored neuronal differentiation in these cells. Thus, Eva1a deletion-induced defective neuronal differentiation is probably associated with a lack of available energy caused by the inhibition of autophagy.

In summary, our results revealed that loss of *Eva1a* leads to impaired NSC self-renewal and differentiation, along with a decrease in autophagy, which is inversely associated with the activation of the PIK3CA/AKT-mTOR signaling. Functionally, EVA1A overexpression or MP treatment substantially rescued *Eva1a*-depletion-induced NSC self-renewal and neuronal differentiation deficiency, demonstrating the crucial function of EVA1A in embryonic

neurogenesis. Our investigations provide insights into the activities of EVA1A, as well as the role of basal autophagy in neurogenesis. Moreover, our results provide a basis for the identification of molecular targets for the treatment of neurodevelopmental disorders caused by dysregulation of autophagy.

EXPERIMENTAL PROCEDURES

Generation of Tissue-Specific *Eva1a*-Deficient Mice

Eva1a$^{flox/flox}$ mice with the C57BL/6J background were constructed by the Model Animal Research Center of Nanjing University (Nanjing, China). Nestin-Cre transgenic mice were provided by Prof. Hong Zhang (Chinese Academy of Sciences, Beijing, China). Progeny containing the *Eva1a* flox allele were bred with these Cre transgenic mice to generate *Eva1a*$^{flox/flox}$; Nestin-Cre mice. All mice used in the study were bred and maintained at the Experimental Animal Center, Peking University Health Sciences Center (Beijing, China). The animal experiment protocol was approved by the Biomedical Research Ethics Committee of Peking University and strictly adhered to the American Physiological Society's *Guiding Principles in the Care and Use of Vertebrate Animals in Research and Training*.

Determination of the Genotype of *Eva1a* Mutant Embryos

To genotype embryos, early-stage embryos' tails were cut and then the genome was genotyped by PCR. The primers used in this study are listed in Table S1.

Protein Extraction and Western Blotting

Total proteins from mouse tissues or cells were extracted using lysis buffer (50 mM Tris [pH 7.4], 150 mM NaCl, 1% Triton X-100, 1% sodium deoxycholate, 0.1% SDS, and with freshly added proteinase inhibitor cocktail and phosphatase inhibitors). Protein concentrations were determined by the BCA protein assay reagent (Pierce, NCI3227CH). Equal amounts of proteins were separated by SDS-PAGE electrophoresis and transferred to nitrocellulose membranes. After blocking with 5% nonfat milk, the membranes were incubated with primary antibodies, washed, and then incubated with the secondary antibodies. The membranes were then washed and scanned using an Odyssey Infrared Imaging System (LI-COR Biosciences). Scanned bands were quantified using the ImageJ software. The results were representative of at least three experiments.

Immunofluorescence

Brain frozen sections from both *Eva1a*$^{-/-}$ and *Eva1a*$^{+/+}$ mice at E12.5 and E16.5 were fixed with 4% formaldehyde, washed with PBS, and blocked with PBS with 5% BSA and 0.25% Triton X-100 at room temperature for 1 hr. The sections were incubated with the indicated primary antibody at 4°C overnight, washed with PBS three times, and incubated with fluorescein isothiocyanates (FITC) or rhodamine-labeled secondary antibodies at 37°C for 1 hr. Nuclei were stained with Hoechst 33342 for 5 min. Finally, immunofluorescence was detected under a confocal fluorescence microscope (LSM 510 Meta plus Axiovert zoom, Carl Zeiss) with a 63×/1.40 NA oil immersion objective lens (PlanApochromat; Carl Zeiss) and a camera (AxioCam HRm, Carl Zeiss). Images were processed and viewed using the LSM Image Browser software.

RT-PCR

Total RNA was extracted from mice tissues or cells using the Trizol reagent (Invitrogen, 15596-026). RT-PCR was performed using 0.1 μg of cDNA with a 2× Taq mastermix (CWBIO, cw0682) and 10 pmol/μl of primers. Reactions were run on a Bio-Rad MyCycler Thermal Cycler, and PCR products were analyzed by agarose gel electrophoresis. The primers used in this study are listed in Table S2.

BrdU Incorporation Assay

Cell proliferation was detected using bromodeoxyuridine (BrdU) (Sigma-Aldrich, B5002). Briefly, BrdU was dissolved in 0.9% sterile NaCl and filtered through a 0.22-μm filter. BrdU was then applied to pregnant female mice by intraperitoneal injection (50 mg/kg) 4 hr before euthanasia. The embryos were removed, and the tail from each embryo was collected for genotyping. The brain of each embryo was immediately fixed in 4% paraformaldehyde. Two days later, the fixed brains were transferred to a solution of 30% sucrose in PBS for cryopreservation. Cryostat sections of the brains were cut in the coronal plane at a thickness of 10 μm and collected on Superfrost Plus slides (VWR). Brain sections were incubated in 2 N HCl at 37°C for 30 min and rinsed in borate buffer (pH 8.5) for 15 min. The sections were then incubated with an anti-BrdU antibody (Bioworld, MB6004) at 4°C overnight after DNA denaturation.

For double labeling of BrdU and NESTIN or β-TUBULIN III, sections were incubated with an anti-BrdU antibody and the indicated antibodies for each cell marker at 4°C overnight after DNA denaturation. Immunofluorescence analysis was performed as described above.

Cell Culture and Treatments

Primary NSCs generated from E12.5 embryos from *Eva1a*$^{+/+}$ and *Eva1a*$^{-/-}$ mice were cultured in Dulbecco's modified Eagle's medium (DMEM/F12, GIBCO, 42400-028) supplemented with 2% B27, 20 ng/ml basic fibroblast growth factor (bFGF) and epidermal growth factor, 100 U/ml penicillin, 100 μg/ml streptomycin, and 2 mM glutamine. Cells were resuspended in DMEM/F12 medium, and then plated onto uncoated tissue culture dishes at 3.5×10^4 cells/cm^2 and incubated at 37°C in 5% CO_2.

To induce cell differentiation, neurospheres from cultures of less than ten passages were plated at a density of 10^5 cells/cm^2 on coverslips coated with 15 mg/ml poly-ornithine (Sigma-Aldrich, P4957), supplemented with N2 (Gibco BRL, 17502048) containing 0.5 μM all-*trans* retinoic acid (Wako, R117), 0.5% fetal bovine serum without bFGF, and incubated for 6 days. The medium was replaced every 2 days.

To study the correlation between energy availability and neuronal differentiation, 10 mM methylpyruvate was added to the culture medium for 6 days. The culture medium was supplemented with 1.5 mg/ml sodium bicarbonate to maintain the pH balance in the presence of MP, and replaced every 24 hr. Cells were then fixed for immunofluorescence or lysed for western blotting.

To detect LC3B distribution, NSCs from *Eva1a*$^{+/+}$ and *Eva1a*$^{-/-}$ at E12.5 were cultured under proliferative conditions and plated on glass coverslips coated with poly-ornithine for 24 hr. NSCs were subjected to immunofluorescence against LC3B and viewed under a confocal fluorescence microscopy.

The recombinant viral plasmid *Ad5-Eva1a* was prepared by Sino-GenoMax. NSCs were infected by incubation with *Ad5-Eva1a* for 12–16 hr, and then fixed for immunofluorescence or lysed for western blotting.

Neurosphere Formation Assay

We collected NSCs on culture day 3 and dissociated them using a NeuroCult cell dissociation kit (Stem Cell Technologies, 05707), and cultured them in 96-well non-coated plates with 500 or 1,000 cells per well. Analyses were performed after 5–7 days in culture. Images of neurospheres (NSs) in 8 wells per experimental condition were acquired and analyzed using ImageJ software to quantify both the number of NSs and the diameter of individual NSs. All data presented are the results of three to four separate experiments.

Measurement of Neurite Length

To visualize neuronal morphology, cells were stained with anti-β-TUBULIN III antibodies, followed by incubation with Texas Red secondary antibody (Molecular Probes, T2767) or with Alexa 488 antibody (Molecular Probes, A1101). Cell nuclei were counterstained with Hoechst 33342. Neurites were classified as primary (predominant processes emerging directly from the cell body) or secondary (processes emerging from a primary neurite). Images of the cells were taken at 40× or 63× magnification using a confocal laser scanning microscope (Olympus). Thirty visual fields were chosen randomly and 30 individual images were taken from each group. Neurite length was measured using the NIH ImageJ software.

Apoptosis Detection

Apoptosis in tissue was detected using an In Situ Cell Death Detection Kit (Roche, 1168479591) by TUNEL assays. Brain frozen sections from both *Eva1a*$^{-/-}$ and *Eva1a*$^{+/+}$ mice at E12.5 were treated and stained according to the manufacturer's directions. The nuclei were stained with Hoechst 33342 and imaged under a confocal microscope. The percentage of TUNEL-positive cells was calculated as the mean of ten different fields from each specimen.

Cell apoptosis was detected by flow cytometry. Primary NSCs generated from *Eva1a*$^{-/-}$ and *Eva1a*$^{+/+}$ mice at E12.5 were cultured in Dulbecco's modified Eagle's medium for 3 days, trypsinized, and resuspended in 100 μl of binding buffer containing 5 μl of FITC-conjugated Annexin V, and incubated at room temperature in the dark for 30 min. The cells were stained with propidium iodide and analyzed on a FACS Calibur flow cytometer (Becton Dickinson).

Statistical Analysis

The statistical significance of the mean differences observed between samples was determined by the Student two-tailed t test using SPSS 18.0. One-way ANOVA with Tukey's post hoc test was used to compare means of more than three samples using SPSS 18.0. Data are shown as means ± SD of the results of at least three independent experiments. Values of $p < 0.05$ were considered significant.

SUPPLEMENTAL INFORMATION

Supplemental Information includes Supplemental Experimental Procedures, four figures, and two tables and can be found with this article online at http://dx.doi.org/10.1016/j.stemcr.2016.01.011.

AUTHOR CONTRIBUTIONS

Conceptualization: Y.B. and Y.C; Methodology: M.L., G.L., J.H., and X.S.; Analysis: M.L., G.L., and X.S. Resources: J.J., Y.G., L.Q., and Y.X. Writing: Y.B., Y.C., and G.L.

ACKNOWLEDGMENTS

We would like to thank Ming Cheng for technical help with the transmission electron microscopy. This work was supported by the National Key Basic Research Program of China (2011CB910103, 2015CB964501), the National Natural Science Foundation of China (31571052, 81272432, 81570235), and Beijing Natural Science Foundation (5162014).

Received: August 14, 2015
Revised: January 15, 2016
Accepted: January 15, 2016
Published: February 18, 2016

REFERENCES

Cecconi, F., Di Bartolomeo, S., Nardacci, R., Fuoco, C., Corazzari, M., Giunta, L., Romagnoli, A., Stoykova, A., Chowdhury, K., Fimia, G.M., et al. (2007). A novel role for autophagy in neurodevelopment. Autophagy *3*, 506–508.

Chang, Y., Li, Y., Hu, J., Guo, J., Xu, D., Xie, H., Lv, X., Shi, T., and Chen, Y. (2013). Adenovirus vector-mediated expression of TMEM166 inhibits human cancer cell growth by autophagy and apoptosis in vitro and in vivo. Cancer Lett. *328*, 126–134.

Dalby, K.N., Tekedereli, I., Lopez-Berestein, G., and Ozpolat, B. (2010). Targeting the prodeath and prosurvival functions of autophagy as novel therapeutic strategies in cancer. Autophagy *6*, 322–329.

Fimia, G.M., Stoykova, A., Romagnoli, A., Giunta, L., Di Bartolomeo, S., Nardacci, R., Corazzari, M., Fuoco, C., Ucar, A., Schwartz, P., et al. (2007). Ambra1 regulates autophagy and development of the nervous system. Nature *447*, 1121–1125.

Gage, F.H. (2000). Mammalian neural stem cells. Science *287*, 1433–1438.

Gotz, M., and Huttner, W.B. (2005). The cell biology of neurogenesis. Nat. Rev. Mol. Cell Biol. *6*, 777–788.

Hara, T., Nakamura, K., Matsui, M., Yamamoto, A., Nakahara, Y., Suzuki-Migishima, R., Yokoyama, M., Mishima, K., Saito, I., Okano, H., et al. (2006). Suppression of basal autophagy in neural cells causes neurodegenerative disease in mice. Nature *441*, 885–889.

Harris, H., and Rubinsztein, D.C. (2012). Control of autophagy as a therapy for neurodegenerative disease. Nat. Rev. Neurol. *8*, 108–117.

Jaeger, P.A., and Wyss-Coray, T. (2009). All-you-can-eat: autophagy in neurodegeneration and neuroprotection. Mol. Neurodegener. *4*, 16.

Klionsky, D.J., Abdalla, F.C., Abeliovich, H., Abraham, R.T., Acevedo-Arozena, A., Adeli, K., Agholme, L., Agnello, M., Agostinis, P., Aguirre-Ghiso, J.A., et al. (2012). Guidelines for the use and interpretation of assays for monitoring autophagy. Autophagy *8*, 445–544.

Komatsu, M., Waguri, S., Ueno, T., Iwata, J., Murata, S., Tanida, I., Ezaki, J., Mizushima, N., Ohsumi, Y., Uchiyama, Y., et al. (2005). Impairment of starvation-induced and constitutive autophagy in Atg7-deficient mice. J. Cell Biol. *169*, 425–434.

Komatsu, M., Waguri, S., Chiba, T., Murata, S., Iwata, J., Tanida, I., Ueno, T., Koike, M., Uchiyama, Y., Kominami, E., and Tanaka, K. (2006). Loss of autophagy in the central nervous system causes neurodegeneration in mice. Nature *441*, 880–884.

Kuma, A., Hatano, M., Matsui, M., Yamamoto, A., Nakaya, H., Yoshimori, T., Ohsumi, Y., Tokuhisa, T., and Mizushima, N. (2004). The role of autophagy during the early neonatal starvation period. Nature *432*, 1032–1036.

Levine, B., and Klionsky, D.J. (2004). Development by self-digestion: molecular mechanisms and biological functions of autophagy. Dev. Cell *6*, 463–477.

Levine, B., and Kroemer, G. (2008). Autophagy in the pathogenesis of disease. Cell *132*, 27–42.

Li, L., Khatibi, N.H., Hu, Q., Yan, J., Chen, C., Han, J., Ma, D., Chen, Y., and Zhou, C. (2012). Transmembrane protein 166 regulates autophagic and apoptotic activities following focal cerebral ischemic injury in rats. Exp. Neurol. *234*, 181–190.

Lu, G.D., Ang, Y.H., Zhou, J., Tamilarasi, J., Yan, B., Lim, Y.C., Srivastava, S., Salto-Tellez, M., Hui, K.M., Shen, H.M., et al. (2015). CCAAT/enhancer binding protein alpha predicts poorer prognosis and prevents energy starvation-induced cell death in hepatocellular carcinoma. Hepatology *61*, 965–978.

Lv, X., Jiang, H., Li, B., Liang, Q., Wang, S., Zhao, Q., and Jiao, J. (2014). The crucial role of Atg5 in cortical neurogenesis during early brain development. Sci. Rep. *4*, 6010.

Mellen, M.A., de la Rosa, E.J., and Boya, P. (2008). The autophagic machinery is necessary for removal of cell corpses from the developing retinal neuroepithelium. Cell Death Differ. *15*, 1279–1290.

Ming, G.L., and Song, H. (2011). Adult neurogenesis in the mammalian brain: significant answers and significant questions. Neuron *70*, 687–702.

Nassif, M., and Hetz, C. (2011). Targeting autophagy in ALS: a complex mission. Autophagy *7*, 450–453.

Paridaen, J.T., and Huttner, W.B. (2014). Neurogenesis during development of the vertebrate central nervous system. EMBO Rep. *15*, 351–364.

Qu, X., Zou, Z., Sun, Q., Luby-Phelps, K., Cheng, P., Hogan, R.N., Gilpin, C., and Levine, B. (2007). Autophagy gene-dependent clearance of apoptotic cells during embryonic development. Cell *128*, 931–946.

Rosello, A., Warnes, G., and Meier, U.C. (2012). Cell death pathways and autophagy in the central nervous system and its involvement in neurodegeneration, immunity and central nervous system infection: to die or not to die–that is the question. Clin. Exp. Immunol. *168*, 52–57.

Schweichel, J.U., and Merker, H.J. (1973). The morphology of various types of cell death in prenatal tissues. Teratology *7*, 253–266.

Sun, W., Ma, X.M., Bai, J.P., Zhang, G.Q., Zhu, Y.J., Ma, H.M., Guo, H., Chen, Y.Y., and Ding, J.B. (2012). Transmembrane protein 166 expression in esophageal squamous cell carcinoma in Xinjiang, China. Asian Pac. J. Cancer Prev. *13*, 3713–3716.

Tao, M., Shi, X.Y., Yuan, C.H., Hu, J., Ma, Z.L., Jiang, B., Xiu, D.R., and Chen, Y.Y. (2015). Expression profile and potential roles of EVA1A in normal and neoplastic pancreatic tissues. Asian Pac. J. Cancer Prev. *16*, 373–376.

Vazquez, P., Arroba, A.I., Cecconi, F., de la Rosa, E.J., Boya, P., and de Pablo, F. (2012). Atg5 and Ambra1 differentially modulate neurogenesis in neural stem cells. Autophagy *8*, 187–199.

Wang, L., Yu, C., Lu, Y., He, P., Guo, J., Zhang, C., Song, Q., Ma, D., Shi, T., and Chen, Y. (2007). TMEM166, a novel transmembrane protein, regulates cell autophagy and apoptosis. Apoptosis *12*, 1489–1502.

Wang, S., Li, B., Qiao, H., Lv, X., Liang, Q., Shi, Z., Xia, W., Ji, F., and Jiao, J. (2014). Autophagy-related gene Atg5 is essential for astrocyte differentiation in the developing mouse cortex. EMBO Rep. *15*, 1053–1061.

Xie, H., Hu, J., Pan, H., Lou, Y., Lv, P., and Chen, Y. (2014). Adenovirus vector-mediated FAM176A overexpression induces cell death in human H1299 non-small cell lung cancer cells. BMB Rep. *47*, 104–109.

Xu, D., Yang, F., He, H., Hu, J., Lv, X., Ma, D., and Chen, Y.Y. (2013). Expression of TMEM166 protein in human normal and tumor tissues. Appl. Immunohistochem. Mol. Morphol. *21*, 543–552.

Yazdankhah, M., Farioli-Vecchioli, S., Tonchev, A.B., Stoykova, A., and Cecconi, F. (2014). The autophagy regulators Ambra1 and Beclin 1 are required for adult neurogenesis in the brain subventricular zone. Cell Death Dis. *5*, e1403.

Zeng, M., and Zhou, J.N. (2008). Roles of autophagy and mTOR signaling in neuronal differentiation of mouse neuroblastoma cells. Cell Signal. *20*, 659–665.

Zhao, Y., Huang, Q., Yang, J., Lou, M., Wang, A., Dong, J., Qin, Z., and Zhang, T. (2010). Autophagy impairment inhibits differentiation of glioma stem/progenitor cells. Brain Res. *1313*, 250–258.